Cal Poly

Caltech

SCEC
AN NSF+USGS CENTER

UC Irvine

UCLA

UC Santa Barbara

USC

EVALUATION OF SEISMIC DEFORMATION ANALYSIS APPROACHES FOR BRIDGE EMBANKMENTS

Richard Armstrong
Department of Civil Engineering
California State University, Sacramento

A report on research supported by California Department of Transportation

Report GIRS-2024-01
DOI: 10.34948/N3PK5Z

University of California, Los Angeles (headquarters)

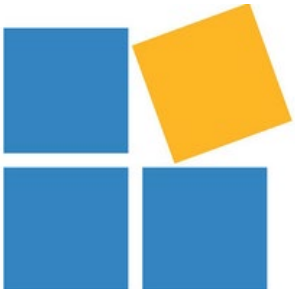

Natural Hazards Risk & Resiliency Research Center

The B. John Garrick Institute for the Risk Sciences

EVALUATION OF SEISMIC DEFORMATION ANALYSIS APPROACHES FOR BRIDGE EMBANKMENTS

A report on research conducted with support from California Department of Transportation

Report GIRS-2024-01
DOI: 10.34948/N3PK5Z

Natural Hazards Risk & Resiliency Research Center
The B. John Garrick Institute for the Risk Sciences
University of California, Los Angeles (Headquarters)

January 2024

ABSTRACT

In this study, nonlinear deformation analyses (NDA) and equivalent-static analyses (ESA) approaches were evaluated for a model bridge embankment that was underlain by a non-liquefiable crust layer, a liquefiable medium dense sand layer, and a non-liquefiable deep dense sand layer. The embankment and underlying ground conditions were selected to represent a scenario when a deformation analysis would be required to assess the impacts of earthquake-induced liquefaction of the ground. Four geometry conditions were considered in the study that differed in the dimensions of the medium dense sand and overlying crust. In addition, two densities of the medium dense sand were considered to assess the impacts of different liquefaction responses. Two earthquake scenarios applicable to California were used, one representing a near-field earthquake scenario and the other representing a far-field earthquake scenario.

Based on the results from the NDA and ESA, it was highlighted that both analysis approaches were able to differentiate similarly between the different model geometries, different medium dense sand densities, and different earthquake scenarios. The magnitude in deformation predicted from the NDA and ESA, however, varied widely. The ESA tended to underpredict displacement when displacements are small and overpredict displacements (i.e., predicting flow failure) when displacements are large. From a practical design standpoint, then, from these results, the ESA appeared sufficient for differentiating between extreme conditions (e.g., deformations very small or very large), but the magnitude of the results themselves lacks accuracy, at least compared to the NDA.

ACKNOWLEDGEMENTS

This study was supported by the California Department of Transportation (Caltrans) and coordinated by the Natural Hazards Risk and Resiliency Research Center (NHR3) headquartered at UCLA. The support is gratefully acknowledged. The findings, conclusions, or recommendations in this publication are those of the authors and do not necessarily represent those of the sponsors.

TABLE OF CONTENTS

LIST OF FIGURES

LIST OF TABLES

1 Introduction

In this study, two seismic deformation analysis approaches were evaluated for a model bridge embankment that was underlain by a non-liquefiable crust layer, a liquefiable medium dense sand layer, and a non-liquefiable deep dense sand layer. The approaches considered were: (1) nonlinear deformation analyses and (2) equivalent-static analyses. Varying ground conditions and ground motions were used in the study to compare the two analysis approaches for a variety of different conditions. Based on the results from each analysis approach, recommendations are made on the relative merits of each for evaluating the performance of bridge embankments in practice.

The embankment and underlying ground conditions were selected to represent a scenario when a deformation analysis would be required to assess the impacts of earthquake-induced liquefaction of the ground. Four geometry conditions were considered in the study and are shown in Figure 1. For these four geometries, the embankment height was set to 24 ft and the dense layer thickness was set to 100 ft. The embankment slope was 2H:1V with a flat approach of 128 ft. A bedrock layer thickness of 6 ft was set for all geometries. Dimensions of the medium dense sand and overlying crust varied between geometries to allow the impacts of changing the thickness and location of the liquefiable medium dense sand to be investigated using the NDA and ESA. For both Geometry 1 and Geometry 2, the thickness of medium dense sand was 12 ft, while the crust thickness was set to 4 ft for Geometry 1 and 12 ft for Geometry 2. Next, for both Geometry 3 and Geometry 4, the thickness of the medium dense sand was changed to 4 ft; the crust thickness was set to 4 ft for Geometry 3 and 12 ft for Geometry 4.

Two earthquake scenarios applicable to California were considered in this study: one representing a near-field earthquake scenario and the other representing a far-field earthquake scenario. For each earthquake scenario, pseudo-spectral acceleration and peak ground velocity targets were estimated. Using these ground motion intensity measure targets, a suite of 11 amplitude scaled motions were developed for each scenario. Thus, in considering the four geometries, two densities of the medium dense sand, and two earthquake scenarios, a total of 16 different analysis models were considered.

The work of this analysis study will now be presented. To begin, the basic properties of the materials modeled are presented in Section 2 along with details on the earthquake scenarios developed and the associated earthquake ground motions. Next, in Section 3, the analysis details and results of the NDA are provided, followed by Section 4, in which the analysis details and results of the ESA are given. In Section 5, NDA and ESA results are compared; in Section 6, final conclusions are made.

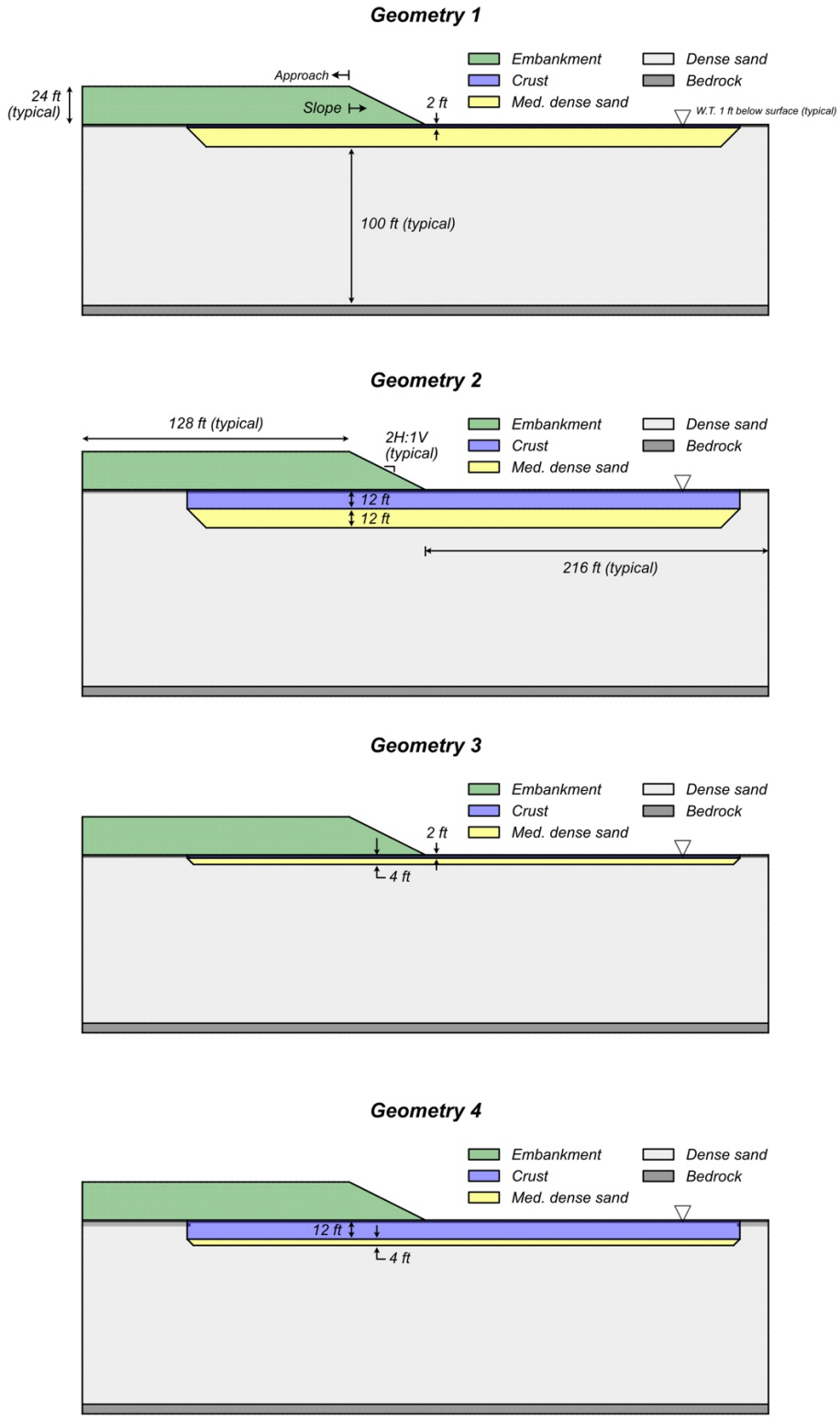

Figure 1: Model study geometries.

2 Material Properties and Earthquake Ground Motions Characterization

2.1 Material Property Selection

Basic properties chosen to represent the different materials in the model are provided in Table 1. For the embankment, properties were selected to represent well-compacted soil; for the dense sand, properties were selected to represent a non-liquefiable granular soil. For the medium dense sand, properties were selected to correspond to two soil densities representative of two different liquefaction responses, one corresponding to a sand with $(N_1)_{60}$ = 8 and the other for a sand with $(N_1)_{60}$ = 14. The non-liquefiable crust properties were selected to be similar to the higher density medium dense sand, but with a model response that will be fully drained throughout earthquake shaking. The bedrock layer was representative of stiff rock.

Table 1: Basic material properties.

Material	Embankment	Crust	Medium dense sand		Dense sand	Bedrock
Unit weight, γ (lb/ft^3)	132	115	115		140	140
Drained friction angle, ϕ' (deg.)	35	33	33		40	---
Normalized SPT value, $(N_1)_{60}$	---	---	8	14	40	---

2.2 Earthquake Ground Motion Characterization

Two earthquake scenarios were developed in this study representative of a near-field and far-field seismic event in California (Table 2). The seismic hazard analysis and selection of earthquake ground motions were conducted by Shantz (2021a) and Shantz (2021b). It is important to note that the ground shaking level was predicted for the bottom of the medium dense sand (top of dense sand layer). The "outcrop" condition, therefore, was for the dense sand with a site class D. The earthquake scenario developed was that of a strike-slip fault. The source-to-site distance for the near-field event was 5 km, and the source-to-site distance for the far-field was 15 km. The epsilon value (ε) for the near-field event was 0.8, and for the far-field event it was ε = 1. Note that when determining the peak ground velocity for the pulse-like near-field ground motions, ε = 1.2. The seismic targets produced are provided in Figure 2 in terms of pseudo-spectral acceleration (PSA, damping ratio of 5%), peak ground acceleration (PGA), and peak ground velocity (PGV).

Table 2: Basic characteristics of two earthquake scenarios.

Metric	Near-field	Farfield
Earthquake magnitude, M_w	7.2	6.7
Peak ground acceleration, PGA (g)	0.58	0.38
Peak ground velocity, PGV (cm/s)	124	50

For the earthquake scenarios, 11 earthquake seed records were selected to represent the near-field earthquake scenario, and 11 earthquake seed records were selected to represent the far-field earthquake scenario. For the 11 near-field earthquake scenarios, six seed records were selected that were non-pulse motions, and five seed records were selected that were pulse motions. The suite of 11 earthquake seed records were subsequently scaled with a scaling factor (SF) such that the mean squared error for spectral periods of 0.01, 0.03, 0.1, 0.32, 1, 2 seconds (equally weighted) were minimized. For each of the 11 ground motions, either the H1 or H2 direction was typically selected. Basic information associated with the 11 ground motions for the near-field and far-field ground motions is provided in Table 3. The ground-motion abbreviations provided in Table 3 will be used throughout this report.

Table 3: Basic ground motion selection and modification information.

GM Abbrev.	Near-field		Far-field	
	NGA-West2 Name	SF	NGA-West2 Name	SF
A	RSN1114_KOBE_PRI000	2.07	RSN1043_NORTHR_NEE180	6.43
B	RSN1120_KOBE_TAK000	0.84	RSN1113_KOBE_OSA000	4.75
C	RSN3748_CAPEMEND_FFS270	1.99	RSN1794_HECTOR_JOS090	2.60
D	RSN4458_MONTENE.GRO_ULO090	2.26	RSN20_NCALIF.FH_H-FRN044	2.18
E	RSN4847_CHUETSU_65010EW	1.55	RSN6036_SIERRA.MEX_RXH-90	8.67
F	RSN4849_CHUETSU_65012EW	3.04	RSN5816_IWATE_48A41EW	2.30
G	RSN6889_DARFIELD_CHHCN01W	3.40	RSN582_SMART1.45_45O08EW	2.45
H	RSN740_LOMAP_ADL250	8.41	RSN6036_SIERRA.MEX_RXH-90	8.67
I	RSN776_LOMAP_HSP000	2.13	RSN756_LOMAP_DFS360	5.17
J	RSN881_LANDERS_MVH135	3.21	RSN757_LOMAP_DUMB267	3.10
K	RSN900_LANDERS_YER270	2.90	RSN884_LANDERS_PSA090	4.14

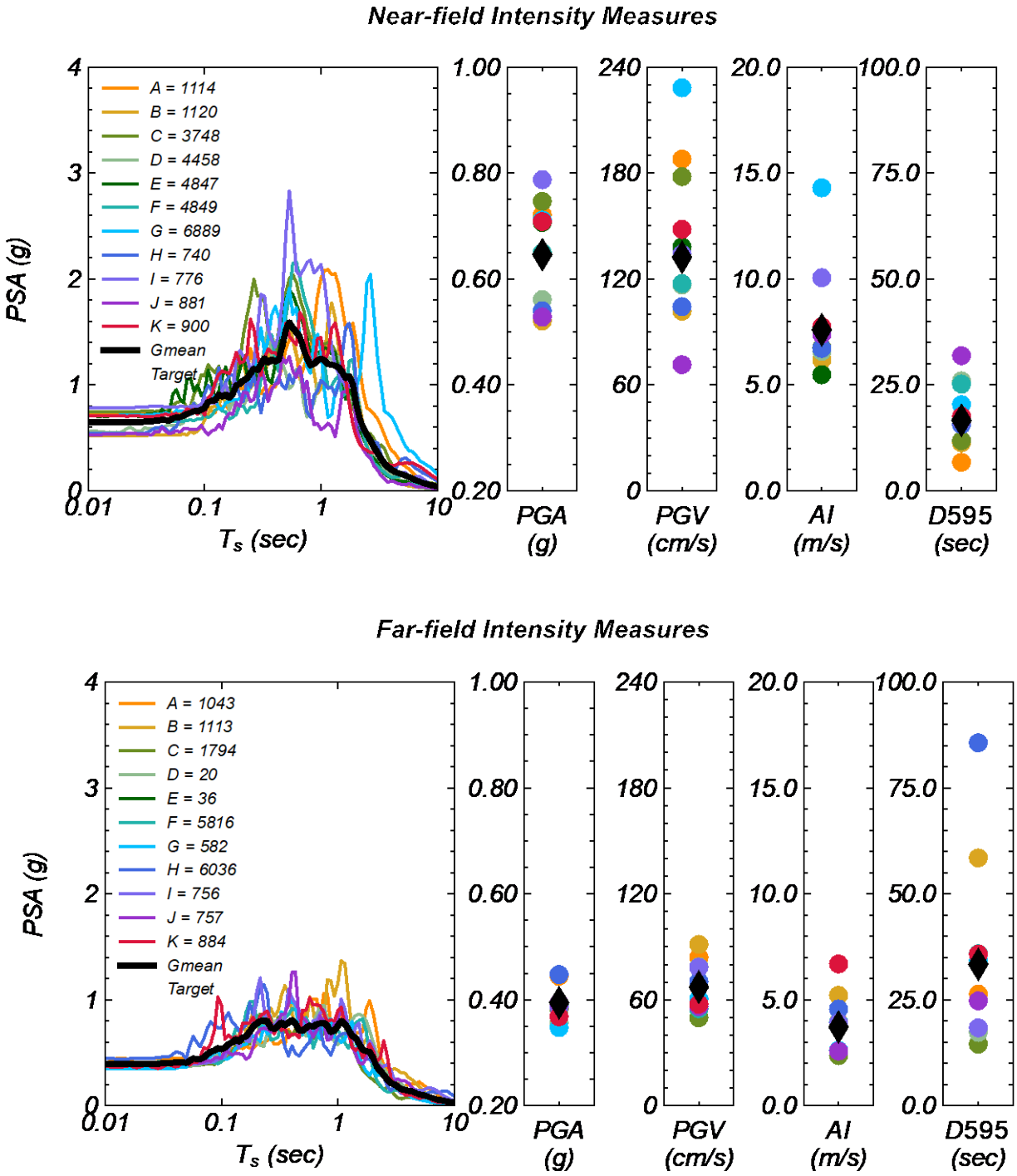

Figure 2: Intensity measures for near-field and far-field earthquake scenarios.

3 Nonlinear Deformation Analyses

3.1 Numerical Analysis Details

For the nonlinear deformation analyses (NDAs), the program FLAC Version 8.1 (Itasca Consulting Group, 2019) was used. FLAC Version 8.1 is a two-dimensional computer software program frequently used in geotechnical engineering practice to predict pre-earthquake stresses, earthquake-induced dynamic responses, and deformations. The software program FLAC was selected because the numerical formulation uses an explicit solution scheme that is well-suited for performing deformation analyses with nonlinear material response, large geometry changes, and instability. For the pre-earthquake analysis, the elastic and Mohr-Coulomb constitutive models were used to calculate the state-of-stress. During earthquake shaking, the UBCHYST model (Byrne and Naesgaard, 2015) was selected to capture the fully drained cyclic response of the embankment, crust layer, and dense sand, and the PM4Sand model (Boulanger and Ziotopoulou, 2017) was selected to capture the liquefaction response of the medium dense sand. Each of the 16 analysis models (i.e., four geometries, two medium dense sand densities, and two earthquake scenarios) were shaken with 11 amplitude scaled ground motions. Thus, a total 4x2x2x11 = 176 NDAs were conducted.

3.2 Material Property Selection

Constitutive model parameters selected for the materials in the NDA are listed in Table 4. These constitutive model parameters relate to elastic moduli, shear strength, stiffness degradation and damping characteristics, and other additional parameters specific to the UBCHYST and PM4Sand constitutive models. The protocol used in this study to select these parameters is similar to Armstrong et al. (2018) and Armstrong et al. (2021). The elastic moduli (e.g., shear modulus, G, and bulk modulus, K) were calculated based on the assumed shear wave velocity (V_s) and drained Poisson ratio (υ') of the materials. Stiffness degradation and damping characteristics were selected to be consistent with the EPRI (1993) G/G_{max} and damping curves. Additional UBCHYST parameters included shear strength $S = \sigma' \sin\phi'$, where ϕ' is the drained friction angle, $\sigma' = \left(\sigma'_x + \sigma'_y\right)/2$ is calculated at each numerical element, and the parameter n (defined based on parameter R) is used to control the hysteretic (i.e., G/G_{max}) behavior. For the PM4Sand model, the three key parameters, D_r, G_0, and h_{p0}, were selected for the medium dense sand so that the dynamic characteristics, included undrained cyclic shear strength, was similar to that expected for a $(N_1)_{60}$ = 8 and $(N_1)_{60}$ = 14 sand. Note that PM4Sand is only able to capture the cyclic mobility response observed with liquefaction (e.g., generation in excess porewater pressure and increasing accumulation of plastic shear strains) and does not model any type of shear strength reduction to a liquefied shear strength such as a residual shear strength (S_r).

Table 4: Material properties used in NDA.

Material	Embankment	Crust	Medium dense sand		Dense sand	Bedrock
Unit weight, γ (lb/ft^3)	132	115	115		140	140
Drained Poisson ratio, ν'	0.30	0.35	0.35		0.30	0.30
Normalized shear wave velocity coefficient, m	0.25	0.25	0.25		0.25	0
Drained friction angle, ϕ' (deg.)	35	33	33		40	---
UBCHYST fitting parameter, R(2)	4000	3000	---		1500	---
Normalized SPT value, $(N_1)_{60}$	---	---	8	14	40	---
Norm. shear wave velocity, V_{s1} (ft/s)	700	562	500(1)	562(1)	800	3000
Relative density, D_r(3)	---	---	0.42	0.55	---	---
Shear modulus coefficient, G_0(4)	---	---	541	678	---	---
Contraction rate parameter, h_{p0}(5)	---	---	0.47	0.41	---	---
Normalized cyclic strength resistance, $CRR_{\sigma'=0,\alpha=0,M=7.5}$(6)	---	---	0.10	0.15	---	---
Target G/G_{max} & ξ curves	EPRI 1993 (0 - 20 ft)	EPRI 1993 (20 - 50 ft)	EPRI 1993 (20 - 50 ft)		EPRI 1993 (50 - 100 ft)	EPRI 1993 (50 - 100 ft)
Constitutive model for dyn. analysis	UBCHYST	UBCHYST	PM4Sand		UBCHYST	UBCHYST

Notes:
(1) Estimated from $(N_1)_{60}$ using $V_{s1} = 279 \times ((N_1)_{60} + 2.5)^{0.25}$
(2) $n = R \times S/G_{max}$ in UBCHYST to achieve target G/G_{max}
(3) Estimated from $(N_1)_{60}$ using $D_r = \sqrt{(N_1)_{60}/46}$, used as parameter in PM4Sand
(4) Estimated from $(N_1)_{60}$ using $G_0 = 167 \times ((N_1)_{60} + 2.5)^{0.5}$, used as parameter in PM4Sand
(5) Calibrated with PM4Sand such that undrained single element test γ = 3% with $CSR = CRR$ is reached in 15 cycles
(6) Estimated from Idriss and Boulanger (2008)
(7) Parameter used in slope stability analyses only. PM4Sand does not use residual strength as model parameter.

3.4 Numerical Mesh Development

Numerical meshes were developed for each of the four geometries (Figure 3). Element sizes were selected to capture important changes in assigned values (e.g., shear modulus), calculate values (e.g., shear strain), and accurately model vertical wave propagation (i.e., element size less the one-tenth the smallest wavelength of interest). In the embankment, dense sand, and bedrock, element sizes were very similar between geometries, but in the crust and medium dense sand, element sizes varied because of the different dimensions. Also in the medium dense sand, it was very important that enough elements in the vertical direction were included to model the variation in excess porewater pressure and associated accumulation of shear strains calculated during shaking.

2.4 Pre-Earthquake Analyses

The effective stresses before the earthquake were calculated because the pre-earthquake state-of-stress affects both initial conditions for the dynamic analysis and the material properties (e.g., elastic stiffness and shear strength). Total stresses for the embankment were estimated by sequentially adding rows of elements of the mesh and solving for static equilibrium with each new row of elements. This process was continued for the entire embankment. The goal of this process was to roughly mimic the actual construction process. Hydrostatic porewater pressures were assigned to the model, and the effective stresses were recalculated.

2.5 Earthquake Analyses

For each earthquake analysis, earthquake shaking was applied as a shear stress time history based on the numerical model, along with a "quiet" boundary to model the impacts of the elastic half space below the model. Along the vertical boundaries, a "free-field" condition was added to simulate the impacts of the free-field soil condition on the model.

The amplitude-scaled ground motions that were developed needed to be adjusted before application at the base of the numerical mesh because the ground motions were developed for the bottom of the medium dense sand (top of dense sand). To modify the ground motions, a series of numerical analyses were conducted in which the embankment, crust, and medium dense sand were removed, and the base motion changed iteratively until the motion calculated at the top of the dense sand layer (now the surface layer) was near the initial target. The velocity time history of this adjusted record was then applied as a shear stress history to model horizontal shaking. No vertical shaking was applied in the analyses.

A small proportion of Rayleigh damping was used in the materials to capture small strain damping characteristics as well as to reduce numerical noise. A representative bulk modulus of porewater fluid was assigned to the medium dense sand so that changes in porewater pressure during shaking were calculated. The "flow-off" condition was used in FLAC. This "flow-off" condition will model undrained response in the medium dense sand with no dissipation of excess pore water pressure due to water flow.

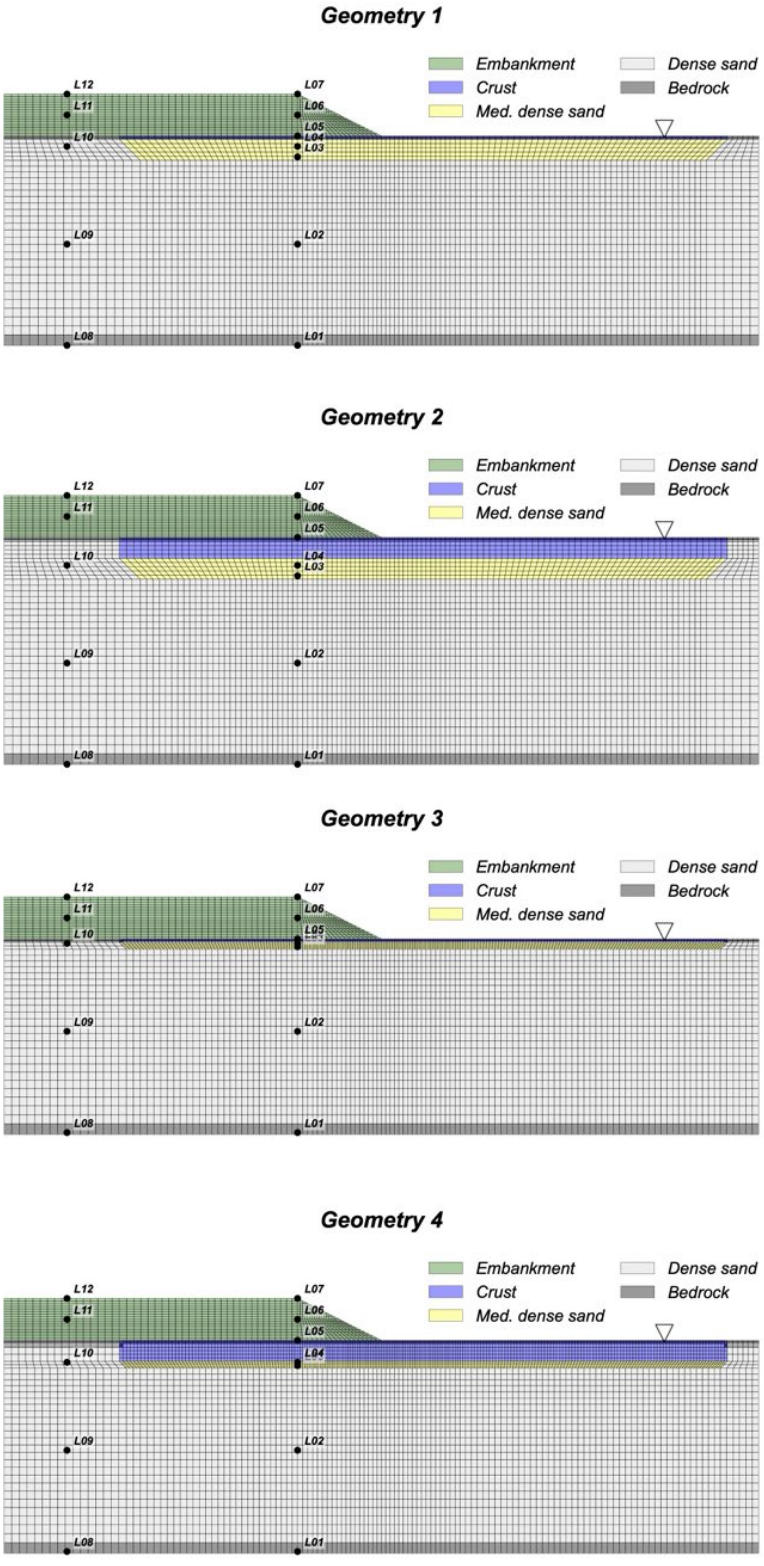

Figure 3: NDA mesh for four model geometries.

2.5 Results

Summary results for the NDA analyses are provided in Table 5, as well as in Figures 4 and 5. In reporting, the results for the four geometries were termed G1, G2, G3, and G4, and the two densities of medium dense sand were termed N8 and N14. In Table 5, only the mean results for the entire suite of near-field and far-field ground motions were provided. The results summarized in Table 5 are representative of the entire triangular embankment slope (representative of the mean values for all elements or nodes contain therein). The properties reported in Table 5 include shear strain increment ($SSI = \frac{1}{2}\left((\varepsilon_x - \varepsilon_y)^2 + 4\varepsilon_{xy}{}^2\right)^{1/2}$), displacement magnitude ($|D| = \left(D_x^2 + D_y^2\right)^{1/2}$), peak horizontal acceleration (PHA), and peak horizontal velocity (PGV).

Vectors of mean $|D|$ are included for the four geometries in Figures 4 and 5, and the contour of SSI will be presented later with the ESA results. Contours of excess porewater pressure ratio (r_u) are not provided, but it was observed that the excess porewater pressure ratio (r_u) reached (or neared) 100% throughout the medium dense sand for both earthquake scenarios.

Table 5: Embankment slope results from NDA with near-field and far-field earthquakes.

Model	Near-field				Far-field			
	SSI (%)	$\|D\|$ (ft)	PHA (g)	PHV (cm/s)	SSI (%)	$\|D\|$ (ft)	PHA (g)	PHV (cm/s)
G1N8	11.1	20.9	0.47	150	6.7	11.8	0.37	83
G1N14	10.6	14.3	0.54	145	5.0	5.8	0.40	78
G2N8	7.1	20.2	0.40	145	6.1	13.8	0.36	83
G2N14	7.0	15.8	0.45	144	4.%	9.0	0.37	82
G3N8	8.9	14.6	0.47	149	4.4	6.9	0.35	81
G3N14	9.6	11.4	0.51	149	4.2	3.7	0.37	74
G4N8	5.8	14.8	0.45	147	4.0	9.1	0.38	81
G4N14	6.2	12.3	0.47	147	3.7	6.1	0.40	79
Mean	8.3	15.5	0.47	147	4.9	8.3	0.37	80
COV	0.246	0.219	0.091	0.015	0.214	0.402	0.043	0.038

As seen in Table 5 or in Figures 4 and 5, the relative deformations between geometries, medium sand densities, and earthquake scenarios were as expected. Deformations were larger in the embankment and underlying crust with the 12-ft-thick liquefiable medium dense sand (Geometry 1 and Geometry 2) than with the 4-ft medium dense sand (Geometry 3 and Geometry 4). Deformations were larger with the near-field earthquake than the far-field earthquake.

As seen in comparing the coefficient of variation (COV), the variation in the inertia loads in the embankment was much smaller than variation in deformations. Also, focusing on the magnitude of the inertia loads (in term of PHA and PHV), PHA was consistently less than the target (PGA = 0.58g for near-field and PGA = 0.38 for far-field), while PHV was consistently larger (PGV = 124 cm/s for near-field and PGV = 50 cm/s for far-field). The topic of the inertial loads in the embankment will be revisited with the ESA.

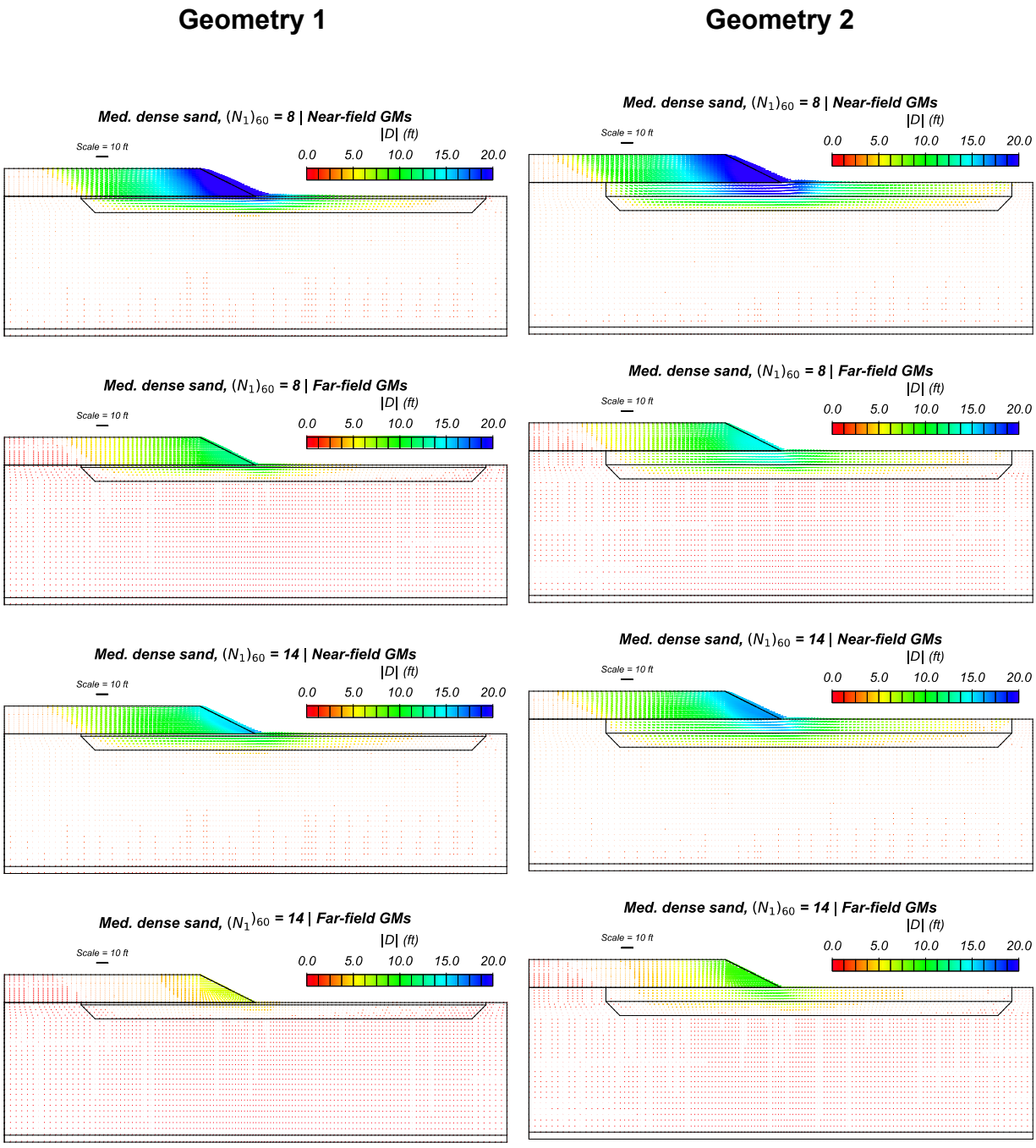

Figure 4: NDA results for Geometry 1 and Geometry 2: mean displacement magnitude.

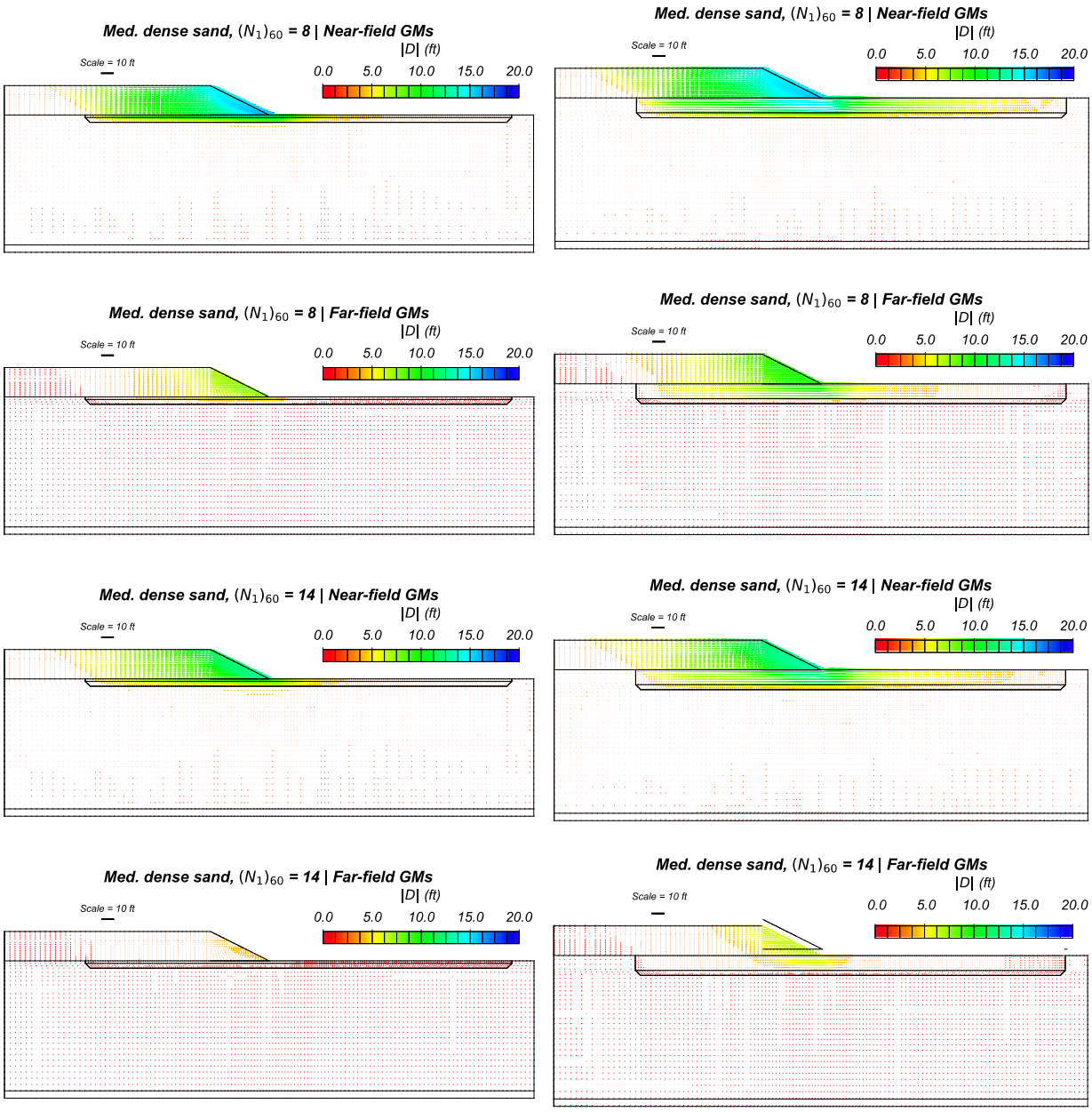

Figure 5: NDA results for Geometry 3 and Geometry 4: mean displacement magnitude.

4 Equivalent-static Analyses

4.1 Numerical Analysis Details

The equivalent-static analyses consisted of determining the seismic yield coefficient for each of the 16 models following by characterizing deformations through Newmark sliding block displacements. The program used to calculate seismic yield coefficients was Slide2D (Rocscience Inc.). Both circular and non-circular slip surfaces were considered in calculating the seismic yield coefficient. Newmark sliding block displacements were estimated using the Bray and Travasarou (2007) and Saygili and Rathje (2008) regression-based sliding block models.

4.2 Material Property Selection

The limit equilibrium analyses conducted in Slide2D required only basic properties (Table 6). Material properties included unit weights and parameters to define the shear strengths. For the embankment, crust, and dense sand, a drained friction angle was used to define a drained Mohr-Coulomb failure criterion according to $\tau = \sigma_n' \tan\phi'$. For the medium dense sand, a residual strength of the soil in a liquefied state (either S_r and S_r/σ_v') was selected using the relationships from Idriss and Boulanger (2008) with $(N_1)_{60}$ equal to 8 or 14. When using S_r, an "undrained failure criterion" was used in Slide2D with $\tau = S_r$, and when using S_r/σ_v', a "vertical stress ratio failure criterion" was used with $\tau = \kappa\sigma_v'$. where $\kappa = S_r/\sigma_v'$.

Table 6: Material properties used in ESA.

Material	Embankment	Crust	Medium dense sand		Dense sand	Bedrock
Unit weight, γ (lb/ft^3)	132	115	115		140	140
Drained friction angle, ϕ' (deg.)	35	33	33		40	---
Normalized SPT value, $(N_1)_{60}$	---	---	8	14	40	---
Residual shear strength, S_r (lb/ft^2)	---	---	182	474	---	---
Residual shear strength, S_r/σ_{v0}'	---	---	0.08	0.12	---	---

4.2 Limit Equilibrium Analyses

Limit equilibrium analyses were conducted in Slide2D for the four geometries. Hydrostatic porewater pressures were assigned. Spencer's method was used to calculate the factor-of-safety (FS) as well as the yield coefficient (k_y). The search method used in Slide2D for circular surfaces was "Auto Refine Search" with composite surfaces. For non-circular slip surfaces, the method used was the "Cuckoo" search with only convex surfaces allowed. Both search methods find the lowest FS or k_y and allow analysis controls so that the slip surfaces found are practically meaningful. The resulting FS and k_y for the different models are reported in Table 7 for the four geometries (G1, G2, G3, and G4) and two densities of medium dense sand (N8 and N14). For models in which a $FS < 1$ was calculated, the k_y is not meaningful.

Table 7: Summary of limit equilibrium results.

Analysis	FS		k_y	
	S_r	S_r/σ'_{v0}	S_r	S_r/σ'_{v0}
G1N8	0.639 (0.473)	0.675 (0.506)	– (–)	– (–)
G1N14	1.015 (0.973)	0.786 (0.683)	0.004 (–)	– (–)
G2N8	1.008 (0.826)	1.153 (1.005)	0.003 (–)	0.014 (–)
G2N14	1.326 (1.210)	1.305 (1.182)	0.068 (0.023)	0.052 (–)
G3N8	0.902 (0.664)	0.821 (0.602)	– (–)	– (–)
G3N14	1.291 (1.164)	0.914 (0.749)	0.114 (0.051)	– (–)
G4N8	1.446 (1.153)	1.491 (0.777)	0.110 (–)	0.124 (0.008)
G4N14	1.673 (1.463)	1.567 (0.087)	0.171 (0.080)	0.150 (0.014)

Notes:
Results based on "Auto" and "Cuckoo" methods in Slide2D for S_r and S_r/σ'_{v0} and presented as "Auto (Cuckoo)".

The slip surfaces of the FS or k_y values underlined in Table 7 are shown in Figures 6 and 7 with the following labels: 1A corresponding to S_r in the medium dense sand with Auto Refine Search; 1B corresponding to S_r in the medium dense sand with Cuckoo Search; 2A corresponding to S_r/σ'_{v0} in the medium dense sand with Auto Refine Search; and 2B corresponding to S_r/σ'_{v0} in the medium dense sand with Cuckoo Search. Also included in Figures 6 and 7 are the contours of mean SSI for the four geometries with the two medium dense sand densities from the NDA. The results from the ESA and NDA will be compared in a subsequent section.

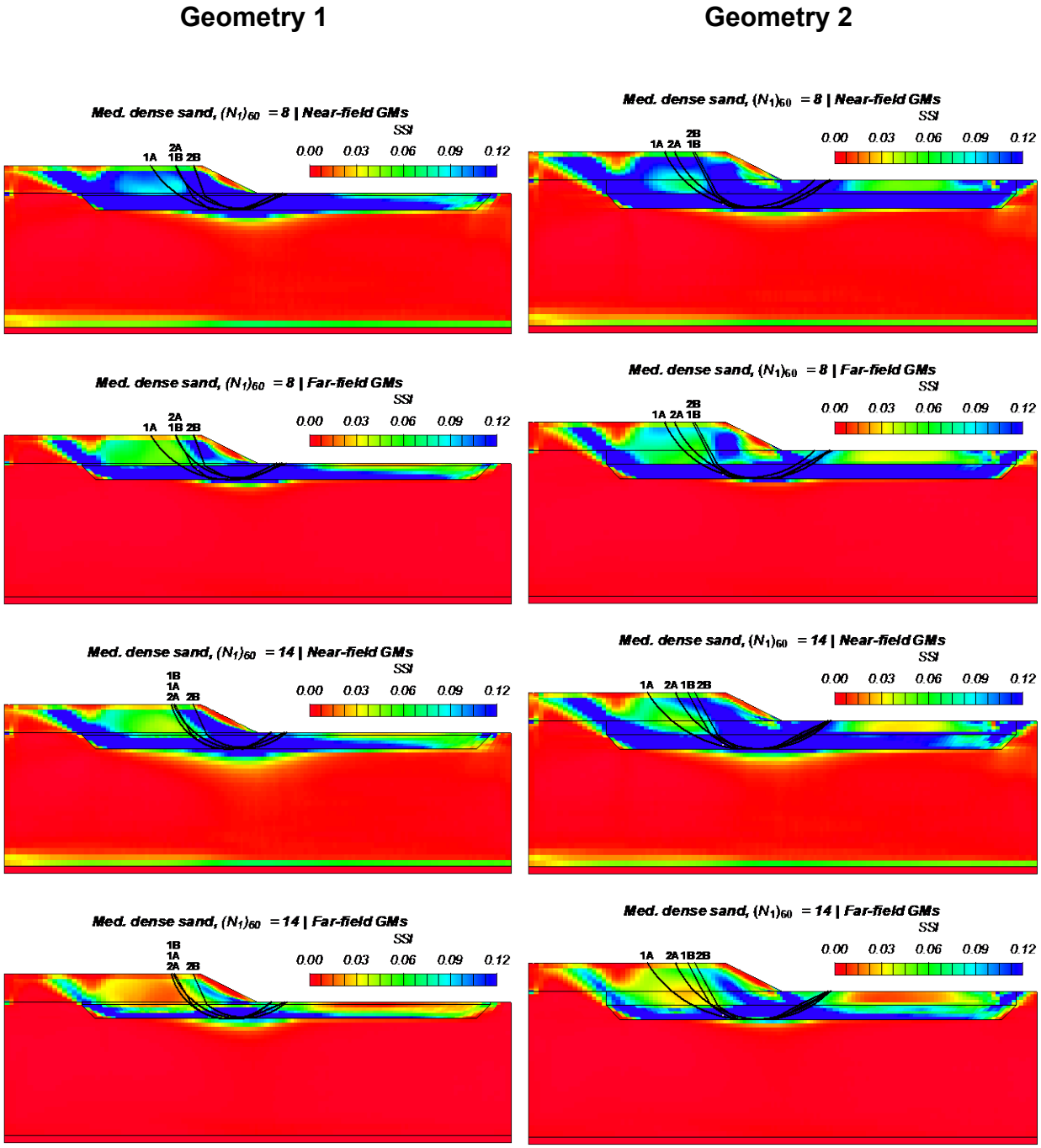

Figure 6: ESA and NDA results for Geometry 1 and Geometry 2.

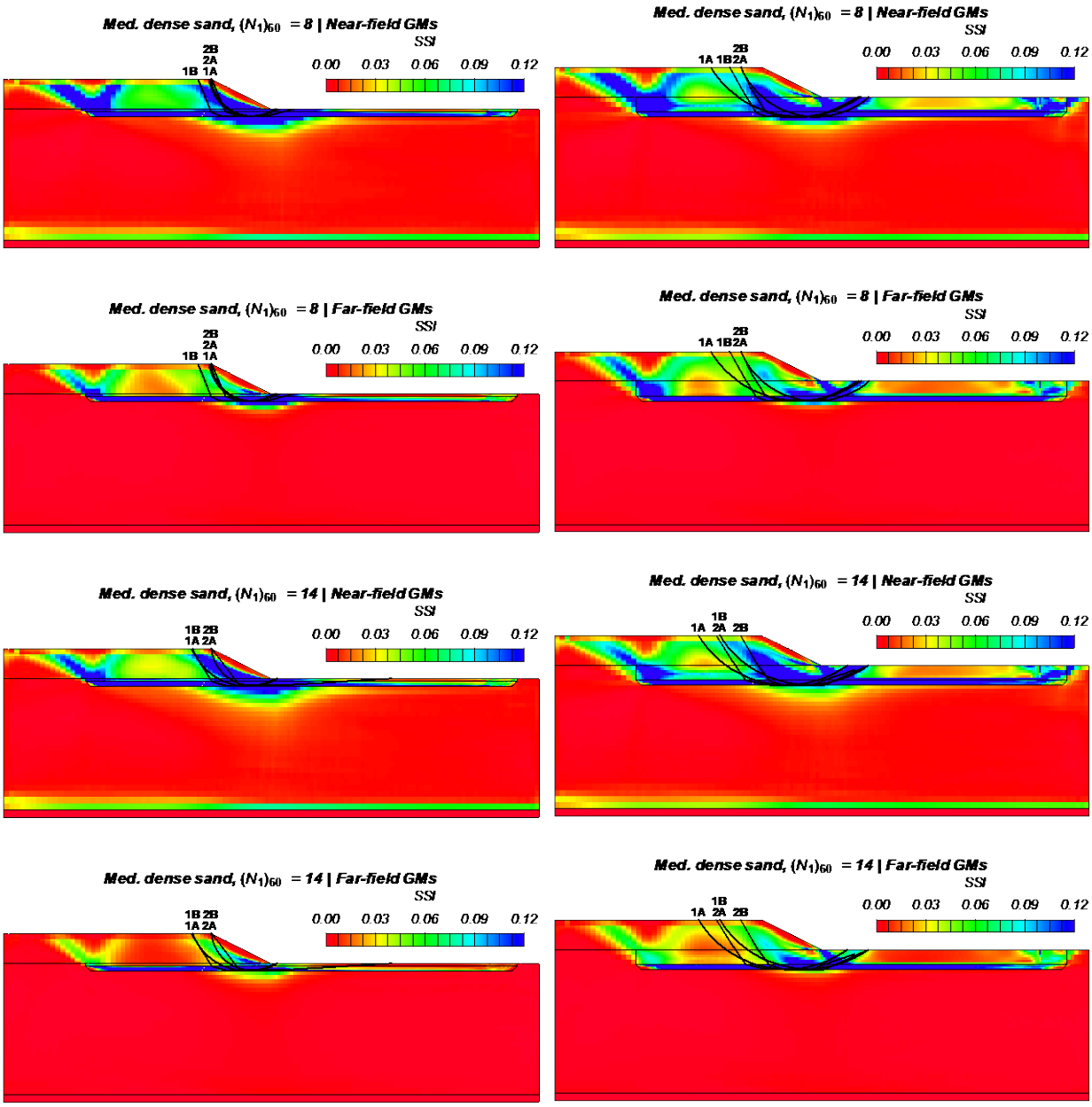

Figure 7: ESA and NDA results for Geometry 3 and Geometry 4.

4.2 Newmark Sliding Block Analyses

Newmark sliding block displacements were estimated using the Bray and Travasarou (2007) – termed here BT07, and Saygili and Rathje (2008) – termed here SR08 – regression-based sliding block models. For the BT07 model, the "rigid block" equation with k_y, PGA, and M_w was used. For SR08 model equation with k_y, PGA, and PGV was used. The Newmark displacements calculated are provided in Table 9 for the near-field earthquake scenario and in Table 10 for the farfield earthquake scenario. For comparison the displacement magnitude of the embankment slope from the NDA is also included. When viewing Table 9 and 10, the term "flow" indicates that the $FS < 1$ was calculated for that model. Newmark sliding block displacements were calculated using the initial seismic hazard target for BT07 and SR08 models. In addition, Newmark displacements were also calculated with SR08 but with a representative value of PHA and PHV from the embankment slope from the NDA. The results from the ESA and NDA will be compared in a subsequent section.

Table 8: Comparison of ESA and NDA results for the near-field earthquake scenario.

Analysis	Target (0.58g | 134 cm/s)				Emb. Slope (0.47g | 147 cm/s)		NDA
	BT07		SR08				
	Auto	Cuckoo	Auto	Cuckoo	Auto	Cuckoo	
Liquefied shear strength in ESA based on S_r							
G1N8	Flow	Flow	Flow	Flow	Flow	Flow	20.9
G1N14	6.5	Flow	16.6	Flow	17.2	Flow	14.3
G2N8	5.4	Flow	16.8	Flow	17.2	Flow	20.2
G2N14	2.1	6.0	8.1	13.9	13.9	19.5	15.8
G3N8	Flow	Flow	Flow	Flow	Flow	Flow	14.6
G3N14	0.9	2.9	4.2	10.1	10.1	12.8	11.4
G4N8	1.0	Flow	4.4	Flow	17.2	Flow	14.8
G4N14	0.4	1.6	1.8	6.8	6.8	7.8	12.3
Liquefied shear strength in ESA based on S_r/σ'_{v0}							
G1N8	Flow	Flow	Flow	Flow	Flow	Flow	20.9
G1N14	Flow	Flow	Flow	Flow	Flow	Flow	14.3
G2N8	4.3	Flow	4.6	Flow	9.5	Flow	20.2
G2N14	1.2	Flow	2.2	Flow	4.5	Flow	15.8
G3N8	Flow	Flow	Flow	Flow	Flow	Flow	14.6
G3N14	Flow	Flow	Flow	Flow	Flow	Flow	11.4
G4N8	0.3	5.2	0.4	5.0	0.9	10.4	14.8
G4N14	0.2	0.2	0.3	0.3	0.5	9.5	12.3

Table 9: Comparison of ESA and NDA results for the far-field earthquake scenario.

Analysis	Target (0.38g | 50 cm/s)				Emb. slope (0.37g | 80 cm/s)		NDA
	BT07		SR08				
	Auto	Cuckoo	Auto	Cuckoo	Auto	Cuckoo	
Liquefied shear strength in ESA based on S_r							
G1N8	Flow	Flow	Flow	Flow	Flow	Flow	11.8
G1N14	5.0	Flow	5.3	Flow	11.0	Flow	5.8
G2N8	4.4	Flow	5.3	Flow	11.2	Flow	13.8
G2N14	0.8	3.0	1.5	3.9	3.2	8.1	9.0
G3N8	Flow	Flow	Flow	Flow	Flow	Flow	6.9
G3N14	0.3	1.2	0.5	2.2	1.1	4.6	3.7
G4N8	0.3	Flow	0.6	Flow	1.2	Flow	9.1
G4N14	0.1	0.6	0.2	1.2	0.3	2.4	6.1
Liquefied shear strength in ESA based on S_r/σ'_{v0}							
G1N8	Flow	Flow	Flow	Flow	Flow	Flow	11.8
G1N14	Flow	Flow	Flow	Flow	Flow	Flow	5.8
G2N8	4.3	Flow	4.6	Flow	9.5	Flow	13.8
G2N14	1.2	Flow	2.2	Flow	4.5	Flow	9.0
G3N8	Flow	Flow	Flow	Flow	Flow	Flow	6.9
G3N14	Flow	Flow	Flow	Flow	Flow	Flow	3.7
G4N8	0.3	5.2	0.4	5.0	0.9	10.4	9.1
G4N14	0.2	0.2	0.3	0.3	0.5	9.5	6.1

5 Comparison of NDA and ESA

In terms of defining the deformation mechanism, the contour of shear strain calculated in the NDA provides a meaningful comparison to the slip surfaces determined in the ESA. As seen in Figures 6 and 7, the ability of the ESA to replicate the areas of highest shear strain varies between geometries. In the NDA, two areas of high shear strain are identified. Both areas pass through the medium dense sand, with one projecting upward near the end of the embankment slope and the other projecting upward near the upslope end of the medium dense sand. For most geometries and medium dense sand densities, the slip surface from the ESA locates closely this area of high shear strain near the slope; however, given that only the most critical slip surface is reported, it does not replicate the area of high shear strain further upslope. Of the four geometries, the slip surface from the ESA is furthest away from the high shear strains near the slope for Geometry 2 (12-ft-thick crust underlain by 12-ft-thick medium dense sand). No specific trends in the location of the slip surface are apparent when comparing those calculated with S_r, or S_r/σ'_{v0} or using the Auto Refine Search or Cuckoo search methods.

The magnitude of deformation varies significantly between the NDA and ESA. As seen in Tables 8 and 9, the ESA tends to underpredict displacement when displacements are small and overpredict displacements (i.e., predicting flow failure) when displacements are large. Of the two methods used to estimate Newmark displacement, SR08 appears to be the preferred approach for a pragmatic point-of-view because of the use of PGA and PGV versus PGA and M_w for BT07. The added flexibility of having PGV as an estimate was useful when predicting Newmark displacements for the near-field earthquake because the PGV estimate includes pulse-effects, whereas the PGA and M_w estimate do not. Also, including the increases in the PGV in the embankment using the results of the NDA, estimating Newark displacements is only possible with the SR08 model.

6 Conclusions

In this study, two seismic deformation analysis approaches were evaluated for a model bridge embankment that was underlain by a non-liquefiable crust layer, a liquefiable medium dense sand layer, and a non-liquefiable deep dense sand layer. The nonlinear deformation analysis approach represented a more realistic representation of the model problem, while the equivalent-static approach represented a more simplified approach that is used more frequently in practice.

Both analysis approaches were able to differentiate similarly between the different model geometries, different medium dense sand densities, and different earthquake scenarios. As an example, both the NDA and ESA similarly predicted that the relative magnitude of deformations (or lack of stability) between the $(N_1)_{60}$ = 8 and 14 in the medium dense and the near-field and far-field earthquake scenarios. In addition, the slip surface from the ESA corresponded well with the locations of high shear strains calculated by the NDA near the slope. The magnitude in deformation predicted from the NDA and ESA, however, varied widely. The ESA tended to underpredict displacement when displacements are small and overpredict displacements (i.e., predicting flow failure) when displacements are large. A critical estimate in the ESA was the residual shear strength (S_r), since this impacts the value of k_y and subsequently the Newmark displacement. Other methods to predict S_r could have been used and may have resulted in a better comparison to the NDA. In comparing any other method to predict S_r, it is important to note the inherit differences between the cyclic mobility liquefaction response being modeled in the NDA to the much more different and simplified response in the ESA and the case-history based approach in which S_r estimates are made.

From a practical design standpoint, then, from these results, the ESA appeared sufficient for differentiating between extreme conditions (e.g., deformations very small or very large), but the magnitude of the results themselves lacks accuracy, at least compared to the NDA. Thus, the displacement demands applied to the bridge superstructure or substructure could differ significantly from those computed from more complex methods such as the NDA.

References

Armstrong, R., Park, D., and Gullen, A. (2018). Cyclic soil behavior of common constitutive models used in non-linear deformation analyses of embankment dams. Proceedings, 2018 Annual United States Society of Dams Conference.

Armstrong, R., Kishida, T., and Park, D. (2021). Efficiency of ground motion intensity measures with earthquake-induced earth dam deformations. *Earthquake Spectra.* 37(1).

Byrne, P.M. and Naesgaard, E. (2015). Personal Communications. UDM Version: 5d. https://www.itascainternational.com/software/udm-library/ (Accessed 12/29/23).

Boulanger, R. W. and Ziotopoulou, K. (2017). "PM4Sand (version 3.1): A sand plasticity model for earthquake engineering applications." Report No. UCD/CGM-17/01, Center for Geotechnical Modeling, Department of Civil and Environmental Engineering, University of California, Davis, CA, 112 pp.

Bray, J. D. and Travasarou, T. (2007). "Simplified procedure for estimating earthquake-induced deviatoric slope displacements." Journal of Geotechnical and Geoenvironmental Engineering, ASCE, 133(4), 381–392.

Electric Power Research Institute (1993). Guidelines for site specific ground motions, Rept. TR-102293, 1-5, Pala Alto, California.

Idriss, I.M. and Boulanger, R.W. (2008). Soil liquefaction during earthquakes. Earthquake Engineering Research Institute. Oakland, CA, 261 pp

Itasca Consulting Group. (2019). FLAC, Fast lagrangian analysis of continua, user's guide, Version 8.0, Itasca Consulting Group, Minneapolis.

Saygili, G. and Rathje, E. (2008). Empirical predictive models for earthquake- induced sliding displacements of slope. J. Geotechnical and Geoenvironmental Eng., ASCE 134(6), 790-803.

Shantz, T. (2021a). Personal Communication. March 31, 2021

Shantz, T. (2021b). Personal Communication. June 14, 2021

Appendix